

# Coupled Channels Marchenko Inversion for Nucleon–Nucleon Potentials

*H. Kohlhoff and H.V. von Geramb*

Theoretische Kernphysik, Universität Hamburg  
Luruper Chaussee 149, D-22761 Hamburg, Germany

**Abstract:** Marchenko inversion is used to determine local energy independent but channel dependent potential matrices from optimum sets of experimental phase shifts.  ${}^3SD_1$  and  ${}^3PF_2$  channels of nucleon–nucleon systems contain in their off–diagonal potential matrices explicitly the tensor force for  $T = 0$  and 1 isospin. We obtain, together with single channels, complete sets of quantitative nucleon–nucleon potential results which are ready for application in nuclear structure and reaction analyses. The historic coupled channels inversion result of Newton and Fulton is revisited.

## 1 Inversion formalism

Marchenko's fundamental equation is here generalized to a system of coupled integral equations in which two partial waves with orbital angular momentum  $\ell_1 = J - 1$  and  $\ell_2 = J + 1$  enter. Such a situation occurs for a neutron–proton pair in the  ${}^3SD_1$ ,  $T = 0$  channel and for proton–neutron, proton–proton or neutron–neutron pairs in  ${}^3PF_2$ ,  $T = 1$  channels. The only bound NN system is the deuteron in a  ${}^3SD_1$  configuration with  $E_B = 2.2246$  MeV binding energy.

With coupled channel inversion we generalize many features which occur with single channel inversions and superficially speaking it requires only to replace the input and output kernels by matrix kernels [1, 2]. For the Marchenko equation this generalization gives

$$\mathbf{A}(r, t) + \mathbf{F}(r, t) + \int_r^\infty \mathbf{A}(r, s) \mathbf{F}(s, t) ds = 0. \quad (1)$$

We use boldface letters to signify matrices where their dimensions are either obvious or shall get well defined in the applications. The input kernel  $\mathbf{F}(r, t)$  is a  $2 \times 2$  matrix with vectors as matrix elements which are functions of  $(r, t)$  and whose rows and columns are indexed by the orbital angular momentum quantum numbers  $(\ell_1, \ell_2) \rightarrow (1, 2)$ . All other quantum numbers, such as  $S$ ,  $J$  and  $T$  are conserved and are suppressed in the expressions. The input kernel contains in

general continuum and  $N_B$  bound states

$$\mathbf{F}(r, t) = \frac{1}{2\pi} \int_{-\infty}^{\infty} \mathbf{H}(kr) [\mathbf{S}^0(k) - \mathbf{S}(k)] \mathbf{H}(kt) dk + \sum_{i=1}^{N_B} \mathbf{H}(i\kappa_i r) \mathbf{N}(\kappa_i) \mathbf{H}(i\kappa_i t). \quad (2)$$

With a centripetal barrier reference potential the reference S-matrix becomes a unit matrix,  $\mathbf{S}^0(k) \rightarrow \mathbf{1}$ , and the diagonal matrix

$$\mathbf{H}(kr) := \begin{pmatrix} (-1)^{\ell_1} h_{\ell_1}(kr) & 0 \\ 0 & (-1)^{\ell_2} h_{\ell_2}(kr) \end{pmatrix} \quad (3)$$

contains outgoing Riccati-Hankel functions as free Jost solutions. The asymptotic bound state normalization matrix  $\mathbf{N}(\kappa_i)$  is determined from physical solutions and Jost solutions to the bound state k-value

$$\Psi_i(r) \Psi_i^\dagger(r) = \mathcal{F}(\kappa_i, r) \mathbf{N}(\kappa_i) \mathcal{F}^\dagger(\kappa_i, r). \quad (4)$$

The inversion potential matrix is related to the output kernel by

$$\mathbf{V}(r) = -2 \frac{d}{dr} \mathbf{A}(r, r). \quad (5)$$

Inserting (5) into the Schrödinger equation

$$\left[ \frac{d^2}{dr^2} - \frac{1}{r^2} \mathbf{L}^2 + k^2 \right] \Psi(k, r) = \mathbf{V}(r) \Psi(k, r) \quad (6)$$

reproduces the original phase shifts for positive energies and bound state properties respectively.

This last point seems trivial, but in practical applications it is very useful and gives a unique possibility to verify results in a closed loop with input data. We find numerically a consistency to within five or six digits.

For single channel inversion we developed an algorithm for rational S-matrix representations which by dint of its construction assured all symmetries and practically any desired accuracy [3, 4]. It is based on Padé approximants for the exponential function and rational function representation of data [5]. A generalization of this algorithm for coupled channel S-matrices was most essential for all our developments and we did not find any alternative working algorithm of a similar power [2].

### 1.1 Marchenko algorithm for rational S-matrices

Rational S-matrices yield finite rank separable input kernels

$$\mathbf{F}(r, t) = \mathbf{F}_I(r) \mathbf{F}_{II}(t) \quad (7)$$

and imply separable output kernels

$$\mathbf{A}(r, t) = \mathbf{A}(r) \mathbf{F}_{II}(t). \quad (8)$$

Insertion of this ansatz into (1) gives a linear equation for the factor matrix

$$\mathbf{A}(r) = -\mathbf{F}_I(r) - \mathbf{A}(r) \int_r^\infty \mathbf{F}_{II}(s) \mathbf{F}_I(s) ds \quad (9)$$

or

$$\mathbf{A}(r) [\mathbf{1} + \mathbf{W}(r)] = -\mathbf{F}_I(r) \quad (10)$$

with

$$\mathbf{W}(r) = \int_r^\infty \mathbf{F}_{II}(s) \mathbf{F}_I(s) ds. \quad (11)$$

Thereby the potential matrix is readily obtained from

$$\begin{aligned} \mathbf{V}(r) = & 2 \mathbf{F}'_I(r) [\mathbf{1} + \mathbf{W}(r)]^{-1} \mathbf{F}_{II}(r) \\ & + 2 \left[ \mathbf{F}_I(r) [\mathbf{1} + \mathbf{W}(r)]^{-1} \mathbf{F}_{II}(r) \right]^2 \\ & + 2 \mathbf{F}_I(r) [\mathbf{1} + \mathbf{W}(r)]^{-1} \mathbf{F}'_{II}(r). \end{aligned} \quad (12)$$

Symmetries of  $\mathbf{S}$  and  $\mathbf{N}$  imply a symmetric input kernel and thus

$$\mathbf{F}(r, t) = \mathbf{F}^T(t, r) \quad (13)$$

or

$$\mathbf{F}_I(r) \mathbf{F}_{II}(t) = \mathbf{F}_{II}^T(r) \mathbf{F}_I^T(t). \quad (14)$$

Resulting from this, the potential matrix

$$\mathbf{V}(r) = \mathbf{V}^T(r) \quad (15)$$

is symmetric and agrees with what is needed in the Schrödinger equation.

Next we discuss some aspects of the S-matrix input. Technically, there are often two possibilities used to factorize bound state poles from the continuum S-matrix. They are equivalent in their final results and are known as single- and double-pole extractions. We realized both options in the computer program but describe only the preferred option herein. Both methods are described and studied with their numerical consequences in [2]. Here we use the rational S-matrix with one bound state at  $E_B = (\kappa)^2$  in partial fraction decomposition, with common poles for any strengths matrix  $\mathbf{S}_i$  and  $\kappa \neq \beta$ , viz.

$$\mathbf{S}(k) = \mathbf{1} + \frac{\mathbf{S}_1}{k - i\kappa} + \frac{\mathbf{S}_2}{k - i\beta} + \sum_{n=3}^{2N+2} \frac{\mathbf{S}_n}{k - \sigma_n}. \quad (16)$$

This representation and analyticity of (3) in (2) allows contour integration with closure in the upper complex k-plane and gives the closed form input kernel

$$\mathbf{F}(r, t) = -i \sum_{n=1}^{N+2} \mathbf{H}(\sigma_n r) \left[ \mathbf{S}_n + i\delta_{1n} \mathbf{N}(\kappa) \right] \mathbf{H}(\sigma_n t). \quad (17)$$

With

$$\text{Res}\{\mathbf{S}(i\kappa)\} = \mathbf{S}_1 = -i\mathbf{N}(\kappa) \quad (18)$$

it is

$$\mathbf{F}(r, t) = -i \sum_{n=2}^{N+2} \mathbf{H}(\sigma_n r) \mathbf{S}_n \mathbf{H}(\sigma_n t). \quad (19)$$

We write this kernel as a product of three matrices

$$\mathbf{F}(r, t) = \mathbf{F}^T(r) \Lambda \mathbf{F}(t) \quad (20)$$

and distinguish

$$\mathbf{F}(r) = \begin{pmatrix} \mathbf{F}_1(r) & 0 \\ 0 & \mathbf{F}_2(r) \end{pmatrix} = \begin{pmatrix} h_{\ell_1}(\sigma_2 r) & 0 \\ \vdots & \vdots \\ h_{\ell_1}(\sigma_{N+2} r) & 0 \\ 0 & h_{\ell_2}(\sigma_2 r) \\ \vdots & \vdots \\ 0 & h_{\ell_2}(\sigma_{N+2} r) \end{pmatrix} \quad (21)$$

and

$$\Lambda = \begin{pmatrix} \Lambda_{11} & \Lambda_{12} \\ \Lambda_{21} & \Lambda_{22} \end{pmatrix} = -i \begin{pmatrix} S_2^{11} & \dots & 0 & S_2^{12} & \dots & 0 \\ \vdots & \ddots & \vdots & \vdots & \ddots & \vdots \\ 0 & \dots & S_{N+2}^{11} & 0 & \dots & S_{N+2}^{12} \\ S_2^{21} & \dots & 0 & S_2^{22} & \dots & 0 \\ \vdots & \ddots & \vdots & \vdots & \ddots & \vdots \\ 0 & \dots & S_{N+2}^{21} & 0 & \dots & S_{N+2}^{22} \end{pmatrix}. \quad (22)$$

Finally, the potential matrix is given by

$$\mathbf{V}(r) = 2 \mathbf{F}^{T'}(r) \mathbf{X}(r) \mathbf{F}(r) + 2 [\mathbf{F}^T(r) \mathbf{X}(r) \mathbf{F}(r)]^2 + 2 [\mathbf{F}^{T'}(r) \mathbf{X}(r) \mathbf{F}(r)]^T \quad (23)$$

with

$$\mathbf{X}(r) = [\mathbf{1} + \Lambda \mathbf{M}(r)]^{-1} \Lambda = [\Lambda^{-1} + \mathbf{M}(r)]^{-1} = \mathbf{X}^T(r) \quad (24)$$

and

$$\mathbf{M}(r) = \begin{pmatrix} \mathbf{M}_{\ell_1}(r) & 0 \\ 0 & \mathbf{M}_{\ell_2}(r) \end{pmatrix} \quad (25)$$

$$\mathbf{M}_{\ell}(r) = \begin{pmatrix} \int_r^{\infty} h_{\ell}(\sigma_2 s) h_{\ell}(\sigma_2 s) ds & \dots & \int_r^{\infty} h_{\ell}(\sigma_2 s) h_{\ell}(\sigma_{N+2} s) ds \\ \vdots & \vdots & \vdots \\ \int_r^{\infty} h_{\ell}(\sigma_{N+2} s) h_{\ell}(\sigma_2 s) ds & \dots & \int_r^{\infty} h_{\ell}(\sigma_{N+2} s) h_{\ell}(\sigma_{N+2} s) ds \end{pmatrix}. \quad (26)$$

We solve a system of inhomogenous linear equations

$$[\mathbf{1} + \Lambda \mathbf{M}(r)] \begin{pmatrix} \mathbf{Y}_1 & \mathbf{Y}_2 \\ \mathbf{Y}_3 & \mathbf{Y}_4 \end{pmatrix} = \Lambda \mathbf{F}(r) \quad (27)$$

for the set  $\{\mathbf{Y}_i\}$  with which the components of the symmetric potential matrix are given by

$$\begin{aligned} V_{11} &= 2 \left\{ 2\mathbf{F}'_1{}^T \mathbf{Y}_1 + (\mathbf{F}'_1{}^T \mathbf{Y}_1)^2 + (\mathbf{F}'_1{}^T \mathbf{Y}_2)^2 \right\} \\ V_{12} = V_{21} &= 2 \left\{ \mathbf{F}'_1{}^T \mathbf{Y}_2 + \mathbf{F}'_2{}^T \mathbf{Y}_3 + \mathbf{F}'_1{}^T \mathbf{Y}_2 (\mathbf{F}'_1{}^T \mathbf{Y}_1 + \mathbf{F}'_2{}^T \mathbf{Y}_4) \right\} \\ V_{22} &= 2 \left\{ 2\mathbf{F}'_2{}^T \mathbf{Y}_4 + (\mathbf{F}'_2{}^T \mathbf{Y}_4)^2 + (\mathbf{F}'_1{}^T \mathbf{Y}_2)^2 \right\}. \end{aligned} \quad (28)$$

## 1.2 Rational representation of S-matrix

A Blatt-Biedenharn or eigenchannel decomposition of the coupled S-matrix

$$\mathbf{S}(k) = \mathbf{S}^{\mathbf{BB}}(k) = \begin{pmatrix} S_{11}(k) & S_{12}(k) \\ S_{21}(k) & S_{22}(k) \end{pmatrix} = \mathbf{R}(k) \tilde{\mathbf{S}}(k) \mathbf{R}^T(k) \quad (29)$$

factorizes the S-matrix into three matrices, the rotation matrix

$$\mathbf{R}(k) := \begin{pmatrix} \cos \epsilon(k^2) & -\sin \epsilon(k^2) \\ \sin \epsilon(k^2) & \cos \epsilon(k^2) \end{pmatrix} \quad (30)$$

and the diagonal eigenchannel matrix

$$\tilde{\mathbf{S}}(k) := \begin{pmatrix} \tilde{S}_1(k) & 0 \\ 0 & \tilde{S}_2(k) \end{pmatrix}, \quad \tilde{S}_\ell(k) := e^{2i\delta_\ell(k)} \quad (31)$$

For the rational representation of all matrix elements of  $\mathbf{S}(k)$ , we combine a symmetric Padé approximant for the exponential function

$$e^z \rightarrow P^{[L/L]}(z), \quad (32)$$

with a rational approximation for the phase functions  $\delta_{1,2}(k)$  and  $\epsilon(k^2)$ .  $L=4$  or  $6$  is used in (32) and was found sufficient in all situations which we encountered with data. It is important to use an exponential function representation also for the trigonometric functions  $\sin z$  and  $\cos z$  since the rotation matrix requires  $\sin^2 z + \cos^2 z = 1$ . With a Padé approximant for the exponential function, of any order  $L$ , this trigonometric relation is identically satisfied.

We do not know of any other algorithm which contains algebraically the possibility to include all symmetries of an S-matrix when the rational functions have very high order. A generalization towards higher dimensions is also obvious and this may become important for future work on coupled reaction channels. A factorization of the rational S-matrix into rational Jost-matrices, which is

needed for Gelfand–Levitan inversion, is also facilitated with this algorithm [6, 7, 8]. As numerical advantage, we found it very important that any determination of polynomial roots was only of low order, generally  $< 20$ . Padé tables for  $\exp z$  are analytic and representations in any form, i.e. partial fractions, are available [2, 3, 5].

Phase shift functions  $\delta_{1,2}(k)$  and  $\epsilon(k^2)$  are fitted with standard rational function fitting routines to the data and with a proper ansatz we can always guarantee the required functional dependence in any domain. More details to this point can be found in [2].

Requirements are

low energy behavior	$\mathbf{S}(k) \xrightarrow{k \rightarrow 0} \mathbf{1} + \mathcal{O}(k^{2\ell+1})$
high energy behavior	$\mathbf{S}(k) \xrightarrow{k \rightarrow \pm\infty} \mathbf{1} + \mathcal{O}(\frac{1}{ k })$
unitarity	$ \mathbf{S}(k)  = 1 \quad \forall k \in \mathcal{R}$
symmetry for $k \rightarrow -k$	$\tilde{S}_\ell(k) \tilde{S}_\ell(-k) = 1 \quad \forall k \in \mathcal{C}$
symmetry for $k \rightarrow -k^*$	$\tilde{S}_\ell^*(-k^*) = \tilde{S}_\ell(k) \quad \forall k \in \mathcal{C}$
Levinson's theorem	$\delta_\ell(-\infty) - \delta_\ell(+\infty) = 2\pi n_\ell$

## 2 Applications

There are many good reasons to use rational S–matrix representations for inversion with Marchenko or Gelfand–Levitan equations. Therewith, input kernels become degenerate, i.e. have a finite rank and are separable, and the fundamental integral equations reduce to systems of linear equations. This is an important technical advantage and together with the need of interpolation and extrapolation of measurements in general, and nucleon–nucleon phase shifts in particular, data are very well described by this class of functions. The resulting inversion potentials are sometimes addressed as Bargmann potentials [1].

Ill posed problems and inversions are closely related and data preparation is an important point here, since therewith we often hit imponderabilities which have no unique experimental or theoretical answer [15]. To overcome the ill posedness in our case, it requires foremost an extrapolation of phase shifts beyond the pion production threshold in a way to maintain the subthreshold validity of the resulting potential for a nonrelativistic quantum mechanics of nuclear structure and reactions. This feedback of high energy extrapolations onto low energy phenomena becomes evident when we calculate off–shell t–matrices. With bremsstrahlung studies we associate some hope to gain experimental control about such influences from the domain of relativistic quantum mechanics but until now all studies are disappointing [9]. Few nucleon systems are an alternative for off–shell t–matrix studies and there exists some enthusiasm to follow this line with the aim to narrow our extrapolation options [10, 11]. Meson exchange potentials show different behaviors towards high energies and are presently of little help. Some QCD calculations can be useful if they predict qualitatively e.g. a repulsive core for all partial waves and this within a certain radial region [12]. The physics behind this brief discussion contains many possibilities for lasting controversies and these will be subject elsewhere.

Our present inversion goal is an energy independent potential for a nonrelativistic Schrödinger equation and thus, from a mathematical point of view, one potential which is valid at all energies from  $0 \rightarrow \infty$ . We realize and keep in mind that a Schrödinger equation is only adequate for physics at energies below 300 MeV and all relativistic effects are swallowed by the effective nature of the potential operator. As a saving grace, experiments show that inelastic channels open very gradually and we expect from this circumstance a smooth decay of validity of our potential well above 400–500 MeV. We interpret inversion potentials as very useful quantitative effective operator for the low energy physics, i.e.  $E < 300$  MeV.

We use inversion which permits a different potential for any partial wave and it is only restricted to belong to the class

$$\int_a^\infty r|V(r)| dr < \infty \quad \text{for any } a > 0.$$

Actually our hadronic potentials decay exponentially towards infinity and show a  $1/r$  singularity at the origin. In case of proton–proton inversion we use the point charge Coulomb potential as reference potential and the inversion equations are properly modified [13]. To have a better control of the potential near the origin requires a more detailed control of phase shift behavior at high energy. We assume a phase shift behavior  $\lim_{k \rightarrow \infty} \delta(k) = \mathcal{O}(1/k)$ , for mixing angles  $\lim_{k \rightarrow \infty} \epsilon(k^2) = \mathcal{O}(1/k^2)$  or  $\lim_{k \rightarrow \infty} \epsilon(k^2) = \text{constant}$ . The latter options show no influence on the potentials [2]. At present we have no arguments for an alternative choice than what is quoted. With several examples and applications we will show how insensitive for observables these choices actually are and we are unable to define error bands of potentials as limits of physics.

It is our interpretation of inversion that it starts with a well understood physics, within and beyond the relevant regions which enter as input data, with the aim to yield mathematically well behaved quantities (operators) for applied physics. For nuclear potentials the applications are nuclear structure and nuclear reactions below pion threshold. In general, it will not be possible to state what is well behaved since applications may have different options and preferences and thus inversion is a tool to tune operators as applications require them. For nucleon–nucleon systems this means, that everyone may ultimately generate his own potential with his choice of data and boundary conditions. With this work we also study rational functions as an option for regularization.

## 2.1 ${}^3SD_1$ -channel results

In Fig. 1 are collected eigenchannel phase shifts of the  ${}^3SD_1$  channel from the most recent and complete phase shift analyses. The figure contains single points as well as curves of phase shift analyses and Paris and Bonn–B potential phase functions for energy intervals  $0 \leq E \leq 300$  MeV (left side) and  $0 \leq E \leq 1000$  MeV (right side). The results show little uncertainty between sources with the exception of the mixing angle  $\epsilon_1(k^2)$  of which potential models [19, 20, 21] show a consistent behavior contrary to phase shift analyses with

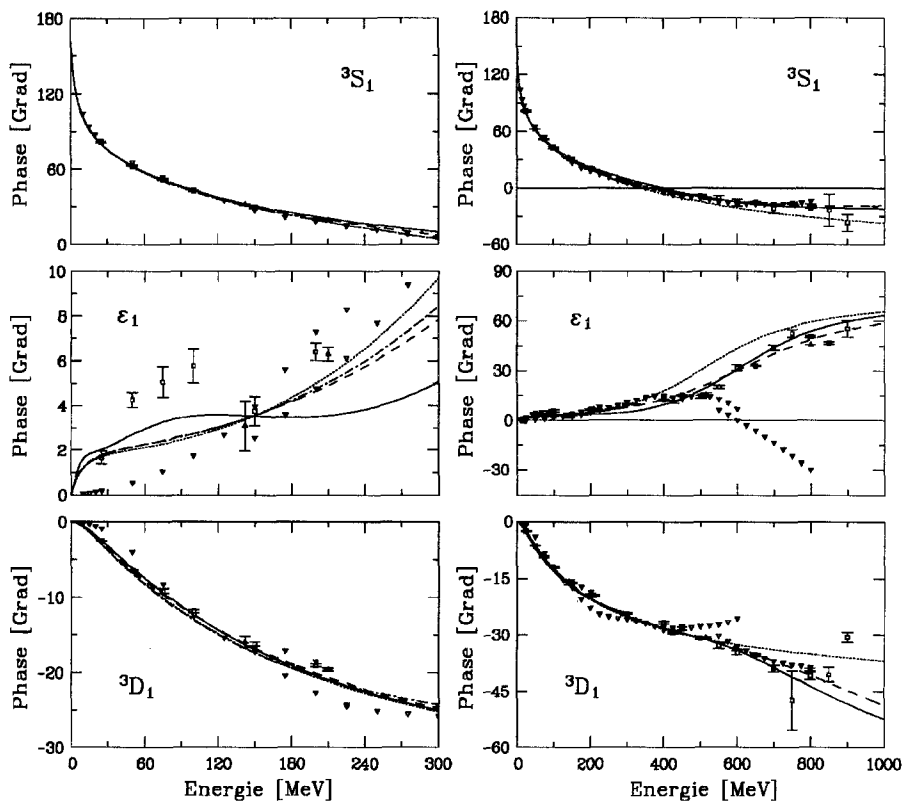


**Fig. 1.** Summary of experimental  ${}^3SD_1$  phase shifts from Virginia [16] (full), Nijmegen [22] (dashed), Saclay [18] (triangles), Arndt single energy data [16] (squares with error bars), Bugg [17] (triangles with error bars), and OBEP theories Paris [19] (dotted), Bonn-B [21] (dash-dotted).

large differences. Particularly at low energy are Saclay data [18] different from other authors.

The uncertainty of the mixing angle is a long standing and often discussed problem and generally it is put equal with an uncertainty of the tensor potential. We shall show that this is insofar not correct as the bound state spectral data, i.e. deuteron binding energy and asymptotic normalization constants, are well determined and this bound state spectroscopic information determines largely the input kernel and thus the coupling potential. More details to this unexpected result can be found in the following.

In Fig. 2 are shown the used phase functions which entered in our calculations and whose potential results are shown in Fig. 3. All important deuteron quantities are listed in Table 1 with used spectroscopic inputs underlined. The qualitative features of the inversion potential matrix agrees well with known results. It comes as a surprise that the coupling potential  $V_{12}(r)$ ,  $r > 1$  fm, is for any of

the chosen input phase shifts closely the same. Their agreement with the genuine Paris and Nijmegen potentials is also visible. At shorter distance,  $r < 1$  fm, the coupling potential is dependent from the high energy,  $E > 300$  MeV, phase shift extrapolations which we do not tune to any specific behavior but allow low energy rational fits to determine them. More details of the tensor potential are shown in Fig. 4. This comparison shows that the regularized Paris tensor force is most consistent with the inversion results.

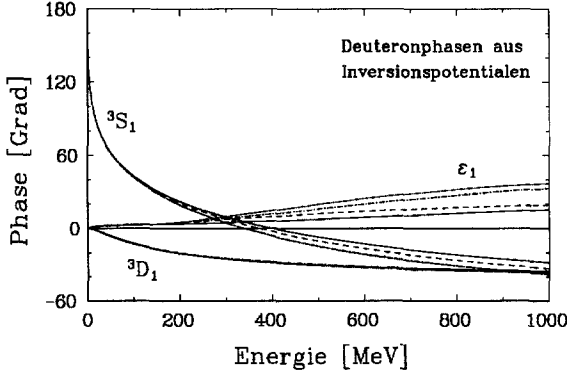


**Fig. 2.** Rational function interpolation phase function to data below 300 MeV from Virginia [16] (full), Nijmegen-3 [22] (dashed), Paris [19] (dotted), Bonn-B [21] (dash-dotted).

Next, we isolate the bound state term in the input kernel Eq. (2) and perform a calculation in which  $\epsilon_1(k^2)$  is put identically to zero. Thus, only the deuteron bound state was allowed to generate a mixing. Table 2 contains the relevant quantities to this calculation which is based on Bonn-B phase shifts. It shows that the D-state probability decreases from 5.86% to 3.69% and similarly the quadrupole moment. The changes of inversion with  $\epsilon \neq 0 \rightarrow \epsilon = 0$  are shown in Fig. 5 and any intermediate results are easy to imagine. In future studies we hope to learn from this example how to increase the sensitivity for an independent determination of  $\epsilon_1(k^2)$  from experiment which requires first to solve the nonlocality problem [23].

Deuteron bound state wave functions are not directly accessible to experiment but are often required in studies of capture or breakup reactions. In Figs. 6 and 7 wave functions of the inversion potentials are shown. Also shown is the variation of the D-state probability

$$P_D(r) := \frac{\int_r^\infty v^2(x) dx}{\int_r^\infty (v^2(x) + w^2(x)) dx}$$

as function of radius in Fig. 6. From this results we conclude that any variation of D-state probability comes from regions with  $r > 1.25$  fm. The momentum

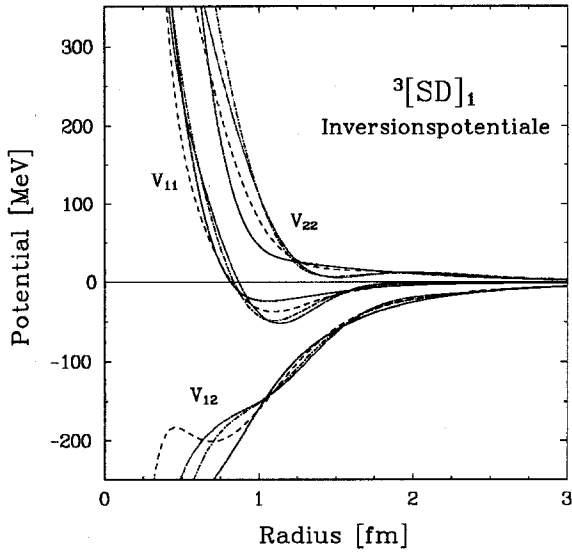


Fig. 3. Inversion potentials, line convention as in Fig. 2.

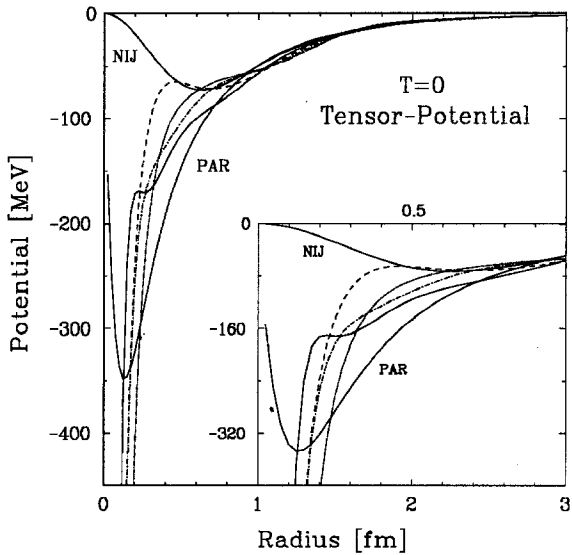


Fig. 4.  $T = 0$  tensor potentials from inversion results of Fig. 3. Also shown are Paris (PAR) [19] and Nijmegen-3 (NIJ) [22] original potentials.

Table 1. Summary of deuteron observables with references.

	INVERSION				EXPERIMENT		THEORY		
	ARN-91	NIJM-3	BONN-B	PARIS	value ( $\pm$ )	Ref.	NIJM-3	BONN-B	PARIS
$E_b$	<u>2.224600</u>	<u>2.224576</u>	<u>2.22465</u>	<u>2.2249</u>	2.22458900 (22)	<sup>a</sup>	2.224575	2.22461	2.2249
$P_D$	6.27	5.53	5.81	5.69	6.0 (2.0)	<sup>b</sup>	5.66	4.99	5.77
					5.0 (2.0)	<sup>c</sup>			
					<5.0 (1.0)	<sup>d</sup>			
$Q_d$	0.2870	0.2705	0.2827	0.2788	0.2859 (3)	<sup>e</sup>	0.2707	0.278	0.279
					0.2860 (15)	<sup>f</sup>			
$\mu_d$	0.8440	0.8482	0.8466	0.8473	0.857406 (1)	<sup>g</sup>	(0.8475)	0.8514	0.853
$A_S$	<u>0.8860</u>	<u>0.8848</u>	<u>0.8861</u>	<u>0.8869</u>	0.8802 (20)	<sup>h</sup>	(0.8847)	0.8860	(0.8868)
					0.8883 (20)	<sup>i</sup>			
					0.8772 (36)	<sup>j</sup>			
					0.8813 (24)	<sup>k</sup>			
					0.8846 (8)	<sup>l</sup>			
$\eta$	<u>0.0264</u>	<u>0.0252</u>	<u>0.0264</u>	<u>0.02608</u>	0.0256 (4)	<sup>m</sup>	0.0252	0.0264	0.02608
					0.0271 (4)	<sup>n</sup>			
					0.0268 (7)	<sup>o</sup>			
					0.0271 (8)	<sup>p</sup>			
					0.0272 (4)	<sup>q</sup>			
					0.0259 (7)	<sup>r</sup>			
					0.02649 (43)	<sup>s</sup>			
$r_{rms}$	1.9748	1.9672	1.9709	1.9716	1.9627 (38)	<sup>t</sup>	(1.9671)	1.9688	(1.9716)
					1.9576 (68)	<sup>u</sup>			
					1.9650 (45)				

<sup>a</sup> Greene G.L. et al., Phys. Rev. Lett. **56**(8), 819 (1986).

<sup>b</sup> Righi S. and Rosa-Clot, M., Z. Phys. A-Atomic Nuclei **326**, 163 (1987).

<sup>c</sup> Ericson T.E.O. and Rosa-Clot M., Ann. Rev. Nucl. Part. Sci. **35**, 271 (1985).

<sup>d</sup> Lomon E.L., Ann. Phys. **125**, 309 (1980).

<sup>e</sup> Bishop D.M. and Cheung L.M., Phys. Rev. **A20**, 381 (1979).

<sup>f</sup> Reid R.V. and Vaida M.L., Phys. Rev. Lett. **34**, 1064 (1975).

<sup>g</sup> Lindgren I., Alpha-, Beta-, Gamma-Spectroscopy, Vol. II, 1620 (1965).

<sup>h</sup> Ericson T.E.O., Nucl. Phys. **A416**, 281 (1984).

<sup>i</sup> Kermode M.W. et al., Z. Phys. **A303**, 167 (1981).

<sup>j</sup> Simon G.G., Schmitt Ch. and Walther V.H., Nucl. Phys. **A364**, 285 (1981), see h.

<sup>k</sup> Berard R.W. et. al., Phys. Lett. **47B**, 355 (1973), see h.

<sup>l</sup> Noyes N.P., Ann. Phys. Nucl. Sci. **22**, 465 (1972), see h.

<sup>m</sup> Rodning N.L. and Knutson L.D., Phys. Rev. Lett. **57**, 2248 (1986).

<sup>n</sup> Klarsfeld S., Matorell J. and Sprung L., Nucl. Phys. **10**, 165 (1984).

<sup>o</sup> Goddard R.P., Knutson L.D. and Tostevin J.A., Phys. Lett. **118B**, 241 (1982).

<sup>p</sup> Borbely I. et al., Phys. Lett. **109B**, 262 (1982).

<sup>q</sup> Gruebler W. et al., Phys. Lett. **92B**, 279 (1980).

<sup>r</sup> Stephenson K. and Haeberli W., Phys. Rev. Lett. **45**, 520 (1980).

<sup>s</sup> Ericson T.E.O., Nucl. Phys. **A416**, 281 (1984).

<sup>t</sup> Simon G.G., Schmitt Ch. and Walther V.H., Nucl. Phys. **A364**, 285 (1981).

<sup>u</sup> Berard R.W. et. al., Phys. Lett. **47B**, 355 (1973).

**Table 2.** Deuteron observables based on inversion potentials with (left column), without (middle column) continuum mixing and with genuine Bonn-B (right column) results. Underlined quantities are inputs.

	$\epsilon \neq 0$	$\epsilon = 0$	BONN-B
$E_b$	<u>2.22461</u>	<u>2.22461</u>	<u>2.22461</u>
$P_D$	5.86	3.69	4.99
$Q_d$	0.2837	0.2524	0.2780
$\mu_d$	0.8463	0.8587	0.8514
$A_S$	<u>0.8860</u>	<u>0.8860</u>	<u>0.8860</u>
$\eta$	<u>0.0264</u>	<u>0.0264</u>	<u>0.0264</u>
$r_{rms}$	1.9708	1.9663	1.9688

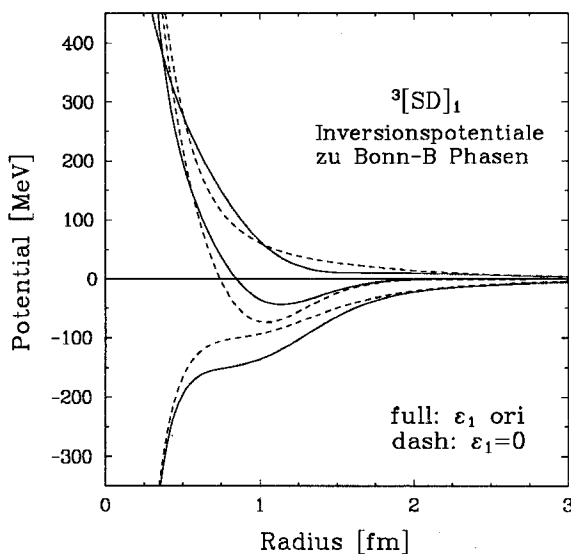


**Fig. 5.** Inversion potentials with (full), without (dashed) continuum mixing. Input phases are from Bonn-B.

space wave functions, Fig. 7, show the expected uncertainty for  $k > 4 \text{ fm}^{-1}$  and there exists no possibility to reduce it even with ideal (low energy) spectral information. High energy  $\gamma + d \rightarrow p + n$  breakup may well be used to sample high momentum components  $k > 4 \text{ fm}^{-1}$  but we don't anticipate a possibility to disentangle complicated mesonic corrections from genuine potential aspects in the wave function.

As last result to the deuteron studies we show effects due to changes/choices in the asymptotic normalization constants with the continuum phase functions fixed. The results are summarized for the Nijmegen-3 phase shifts in Table 3. It

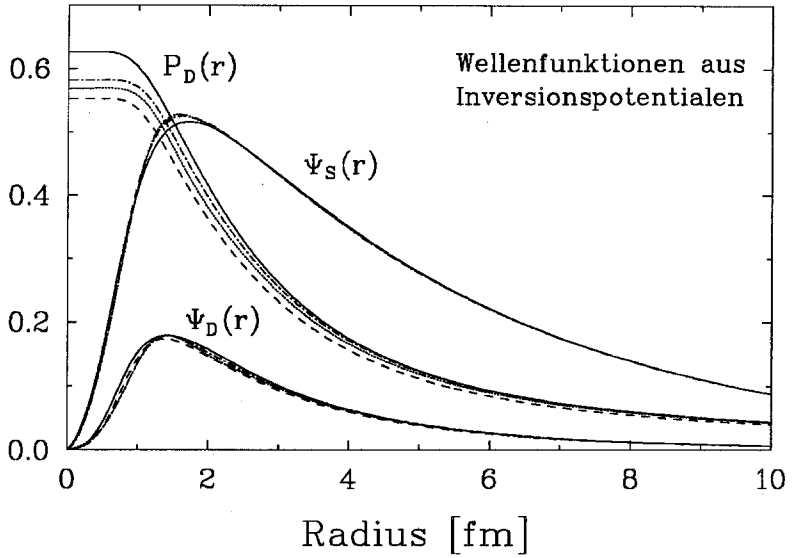


**Fig. 6.** Coordinate space deuteron wave function based on inversion potentials from Fig. 3.  $P_D$  is scaled by a factor 10. Line convention as in Fig. 2

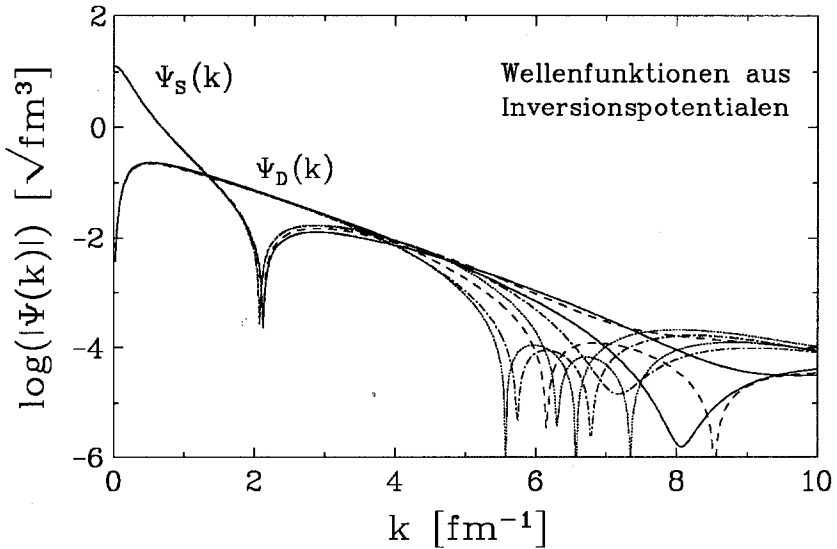


**Fig. 7.** Momentum space deuteron wave function based on inversion potentials from Fig. 3.

**Table 3.** Deuteron observables based on inversion potential to Nijm-3 phase shifts and different asymptotic normalizations. Left column  $A_s = 0.8860$  and  $\eta = 0.0264$ , middle column uses the genuine Nijm-3 asymptotic normalization. Right column values are from [22].

	optimal	Nijm-3	[Sto92]
$E_b$	2.224579	2.224576	2.224575
$P_D$	5.91	5.53	5.66
$Q_d$	0.2816	0.2705	0.2707
$\mu_d$	0.8460	0.8482	—
$A_s$	0.8860	0.8848	—
$\eta$	0.0264	0.0252	0.0252
$r_{rms}$	1.9702	1.9672	—

shows that small variations of the normalization matrix yields significant changes in  $P_D$  and leaves other derived quantities practically unchanged. We conclude from this and other calculations that a very precise D-state probability cannot be found and local potential predictions are expected to give  $P_D = 5.85 \pm 0.3\%$ .

The Nijmegen-3 phase shifts are parametrized via Reid like local potentials for proton-proton and proton-neutron data respectively [22]. The data fit is limited to subthreshold data and the potential thus extrapolates freely towards higher energies. In our extrapolation we are following the trend in Arndt's phase shifts and find thus different potentials, see Fig. 8. This example shows how *inversion* incorporates high energy phase shifts and how difficult it is for *direct* problem solutions. For further details see [2].

## 2.2 Reproductions

Our implementation for the coupled channel Marchenko inversion proves to give excellent reproductions for Yukawa potentials and thereby derived quantities within 5–6 digits and, of a similar quality, for the realistic Bonn-R [20] potential. Such check procedures show different aspects of inversion. 1.) They show how well the whole program works, 2.) it gives many options to see how different energy regions of the input phase functions influence the final potential and this at what radial region. This is a very interesting subject and it will be discussed in more details elsewhere. Some results are contained in [2].

First we assume a superposition of Yukawa potentials which support a bound state in a deuteron like situation. A potential matrix

$$\begin{aligned}
 V_{11}(r) &= 650 \frac{\exp -2r}{r} - 170 \frac{\exp -0.7r}{0.7r} \\
 V_{12}(r) &= V_{21}(r) = -230 \frac{\exp -r}{r} \\
 V_{22}(r) &= 650 \frac{\exp -2r}{r}
 \end{aligned}$$

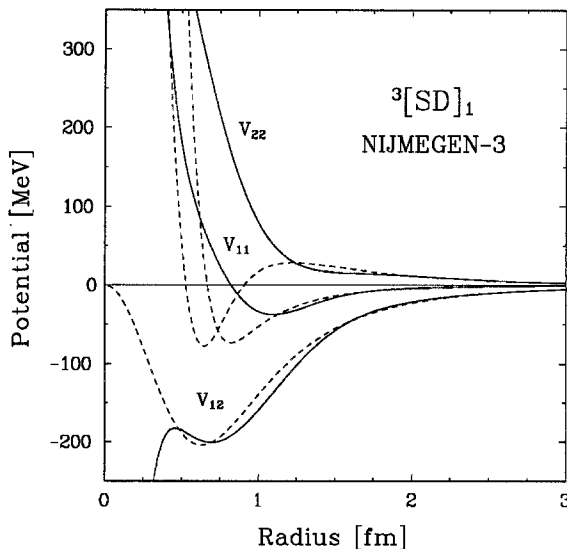


**Fig. 8.** Potentials reproducing Nijmegen phases in the deuteron channels inversion (full) fitted to Nijm-3 phases shifts  $E < 300$  MeV, original Nijm-3 (dashed).

**Table 4.** Reproductions verified with Yukawa and Bonn-R [20] potentials as inputs.

	Yukawa			Bonn-R		
	Inversion	Original	$\Delta$ [%]	Inversion	Original	$\Delta$ [%]
$E_b$	<u>7.009391</u>	<u>7.009636</u>	0.003	<u>2.224534</u>	<u>2.224739</u>	0.009
$P_D$	2.2078	2.2078	0.000	4.680	4.676	0.085
$Q_d$	0.14357	0.14357	0.000	0.2662	0.2671	0.338
$\mu_d$	0.86713	0.86713	0.000	0.8530	0.8531	0.012
$A_S$	<u>1.97801</u>	<u>1.97797</u>	0.002	<u>0.8825</u>	<u>0.8825</u>	0.000
$\eta$	<u>0.02797</u>	<u>0.02797</u>	0.000	<u>0.0253</u>	<u>0.0253</u>	0.000
$r_{rms}$	1.56744	1.56739	0.003	1.9619	1.9638	0.097

is assumed and phase functions are computed for  $0 < E < 3$  GeV. The differences between the input phase shifts and those computed from the inversion potentials are  $< 0.0005^\circ$  for eigenchannel phase functions and  $< 0.03^\circ$  for the mixing angle. The potential reproductions show only the limits of our used numerics with differential equations etc. A realistic potential is the Bonn-R potential and we used it during several stages of our developments but not for our final results since it has little practical importance. The latter potential is parametrized in coordinate space, as the Paris potential, and contains some momentum dependence.

The reproduction is of similar quality as with the Yukawa case and in Table 4 we give the deuteron observables for the two studied examples. The reproduction shows a comparable good agreement. Reproduction checks are routinely performed with all our inversion results.

### 2.3 Newton and Fulton revisited

The first application of quantum inversion to a coupled channel situation of the deuteron was made by Newton and Fulton [24]. Their study gives a striking result for the bound state wave function. Due to a repulsive hump in the tensor component of the potential, for a radius  $r < 1$  fm, the D-wave shows a node near 2 fm. This result is quantitatively changed by a new set of parameters, published a year later [25], but the qualitative behavior remains unaltered.

With this background we attempt a new calculation to the example studied in [24]. When using all parameters of the quoted paper by Newton and Fulton we are able to reproduce their results when: In the phase convention of our implementation we take a *wrong* sign for the mixing angle relative to  $\eta$ . When the *correct* (which we define as ours) phase convention is used, the node in the D-wave disappears and the potentials show the expected behavior. These results give us confidence to claim that a sign error slipped into the historic calculations of Newton and Fulton. However, a definitive localization of the spot, where the error entered, is not possible but we give our arguments and results next.

In the study of Newton and Fulton enters a rational ansatz for the S-matrix, guided by the effective range expansion for the low energy phase shifts, of the form

$$S(k) = \frac{1}{k^4 + 4\chi^4} \begin{pmatrix} 2\chi^2 & k^2 \\ -k^2 & 2\chi^2 \end{pmatrix} \begin{bmatrix} \left(\frac{k+i\phi}{k-i\phi}\right) \left(\frac{k+i\kappa}{k-i\kappa}\right) & 0 \\ 0 & 1 \end{bmatrix} \begin{pmatrix} 2\chi^2 - k^2 \\ k^2 & 2\chi^2 \end{pmatrix}. \quad (33)$$

With the parameter  $\chi$ , the quadrupol moment is fixed, and  $\phi$  and  $\kappa$  dwell upon the effective range expansion of the S-phase and are given by

$$\phi = \frac{1}{r_t} \left( 1 + \sqrt{1 - \frac{2r_t}{a_t}} \right) \quad \text{and} \quad \kappa = \frac{1}{r_t} \left( 1 - \sqrt{1 - \frac{2r_t}{a_t}} \right), \quad (34)$$

where  $a_t$  and  $r_t$  denote triplet scattering length and effective range parameters respectively.

Another parameter  $d$  is introduced with the normalization and is used to fix the D-state probability. The used parameters are  $\kappa = 0.232 \text{ fm}^{-1}$ ,  $\phi = 0.944 \text{ fm}^{-1}$ ,  $\chi = 1.22 \text{ fm}$ ,  $d = 2.27$  leading to 2.08% D-state probability and a quadrupolmoment of  $0.275 \text{ fm}^2$ .

The potential matrix is separated in a form

$$\mathbf{V}(r) = \begin{pmatrix} V_c(r) & \sqrt{8}V_t(r) \\ \sqrt{8}V_t(r) & V_c(r) - 2V_t(r) - 3V_o(r) \end{pmatrix} \quad (35)$$

with  $V_c$ ,  $V_t$ , and  $V_o$  denoting the central-, tensor- and spin-orbit components. They are shown in Figs. 11. For our coupled channel Marchenko inversion a partial fraction representation of the S-matrix is needed. With the definitions

$$\mathbf{S}(k) = \frac{1}{N} \begin{bmatrix} S_{11} & S_{12} \\ S_{21} & S_{22} \end{bmatrix}, \quad S_{12} = S_{21} \quad (36)$$

with

$$\begin{aligned} S_{11} &:= 4\chi^4(k + i\phi)(k + i\kappa) + k^4(k - i\phi)(k - i\kappa) \\ S_{12} &:= 2\chi^2 k^2 [(k - i\phi)(k - i\kappa) - (k + i\phi)(k + i\kappa)] \\ S_{22} &:= k^4(k + i\phi)(k + i\kappa) + 4\chi^4(k - i\phi)(k - i\kappa) \end{aligned}$$

and

$$N = (k - i\phi)(k - i\kappa)(k - \chi(1 + i))(k - \chi(-1 - i))(k - \chi(-1 + i))(k - \chi(1 - i))$$

We get

$$\mathbf{S}(k) = \mathbf{S}^{rat}(k) = \mathbf{1} + \sum_{n=1}^6 \frac{\mathbf{S}_n}{k - \sigma_n} \quad (37)$$

which poles and residues are contained in Table 5.

To determine the normalization matrix  $\mathbf{N}$  we need the asymptotic amplitudes. While  $\eta := A_D/A_S = -0.018081$  is quoted in [24], the value of  $A_S$  is not explicitly given and is here only indirectly determined. We take  $A_S = 0.826$  from the wave function, Fig. 6 in [24], and find good agreement with a value which is given by the rms-radius

$$A_s \simeq 4\sqrt{\kappa^3 r_{rms}} = 0.8269, \quad (38)$$

which is not quite the same value gained from the effective range parameters

$$A_s = \sqrt{\frac{2\kappa}{(1 + \eta^2)(1 - \kappa r_t)}} = 0.8752 \quad (39)$$

or a value determined from the S-matrix

$$A_s = \sqrt{-\text{Im}(S_1^{11})} = 0.8753 \quad (40)$$

Here enters a caveat. While the first two values are derived from the inversion results and the latter are input data, we observe an inconsistency.

Two situations are studied next. In *case (a)* we use the *wrong* sign for the mixing angle, while in *case (b)* the Newton-Fulton parameters are transformed into our *correct* phase convention. The results to *case (a)* are very close to the original Newton and Fulton result.

**Table 5.** Poles and residues for the rational Newton–Fulton S–Matrix.

n	$\Re(\sigma_n)$	$\Im(\sigma_n)$		$\Re(S_n^{ij})$	$\Im(S_n^{ij})$
1	0.000	0.232	$S_1^{11}$	0.0000000000	-0.7661315523
			$S_1^{12}$	0.0000000000	-0.0138525479
			$S_1^{22}$	0.0000000000	-0.0002504702
2	0.000	0.944	$S_2^{11}$	0.0000000000	2.8619074860
			$S_2^{12}$	0.0000000000	0.8567417325
			$S_2^{22}$	0.0000000000	0.2564745366
3	1.22	1.22	$S_3^{11}$	0.5518543198	-0.7000042029
			$S_3^{12}$	-0.7000042029	-0.5518543198
			$S_3^{22}$	-0.5518543198	0.7000042029
4	-1.22	1.22	$S_4^{11}$	-0.5518543198	-0.7000042029
			$S_4^{12}$	0.7000042029	-0.5518543198
			$S_4^{22}$	0.5518543198	0.7000042029
5	-1.22	-1.22	$S_5^{11}$	-0.1304097275	-0.3478837639
			$S_5^{12}$	-0.3478837639	0.1304097275
			$S_5^{22}$	0.1304097275	0.3478837639
6	1.22	-1.22	$S_6^{11}$	0.1304097275	-0.3478837639
			$S_6^{12}$	0.3478837639	0.1304097275
			$S_6^{22}$	-0.1304097275	0.3478837639

**Table 6.** Deuteron observables of the studied cases.

	case (a)	case (b)	[Newton–Fulton]
$E_b$	2.2321397	2.2321399	2.2321394
$P_D$	1.00	6.77	2.09
$Q_d$	0.0925	0.2310	0.275
$\mu_d$	0.8740	0.8412	—
$A_s$	0.8753	0.8753	0.8269
$\eta$	0.018071	0.018081	-0.018081
$r_{rms}$	1.935	1.947	1.85

The D–wave node appears again near 2.8 fm and the repulsive hump in the tensor potential is present. Any remaining quantitative differences are explained with somewhat different input, e.g. we used  $A_s = 0.8753$ .

Case (b) gives results which show the expected potential and bound state wave function. In Table 6 we compare cases (a), (b) and original results. Notice, the quadrupole moment changes in case (b) to a physically better value and  $P_D$  changes from 1.0% to 6.77%. The latter value is in good agreement with today's suggested value.

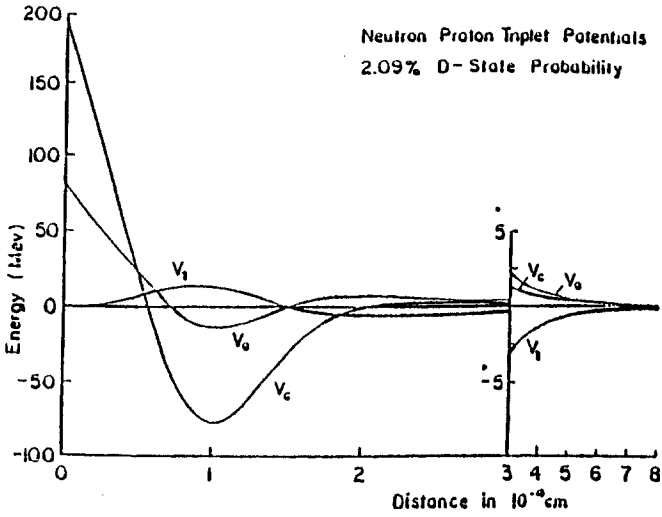


Fig. 9. Original deuteron potential from Newton and Fulton [24].

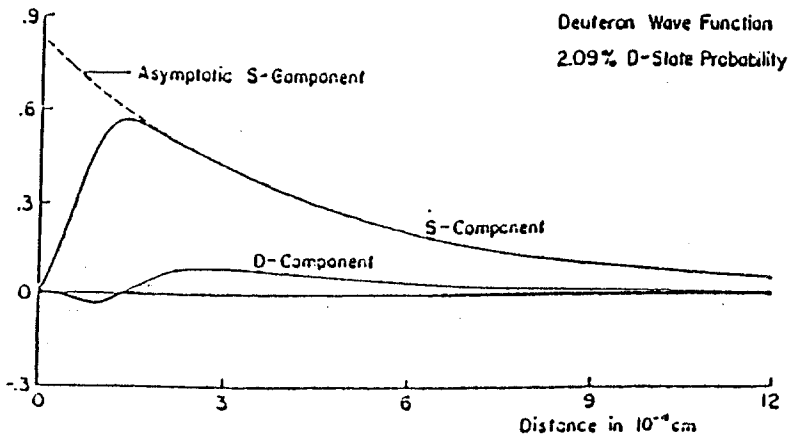


Fig. 10. Original deuteron wave function, from Newton and Fulton [24].

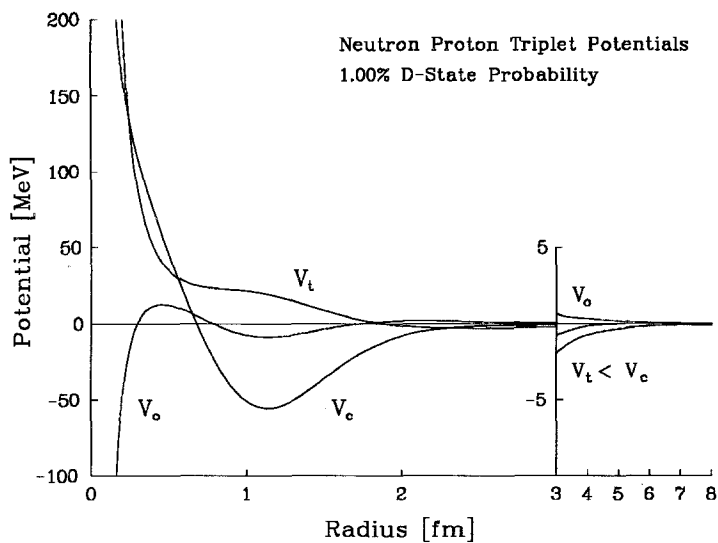


Fig. 11. Inversion potential of Newton and Fulton S-matrix with *wrong sign*, case (a)

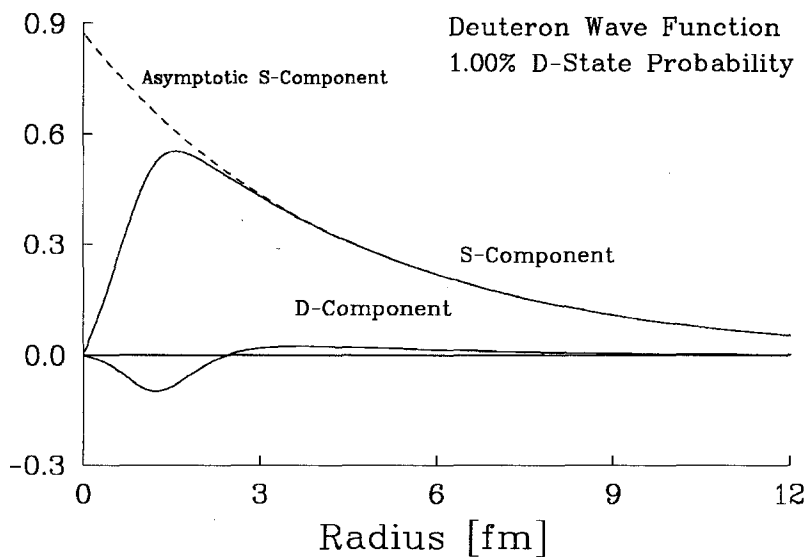


Fig. 12. Deuteron wave function of *case (a)* inversion

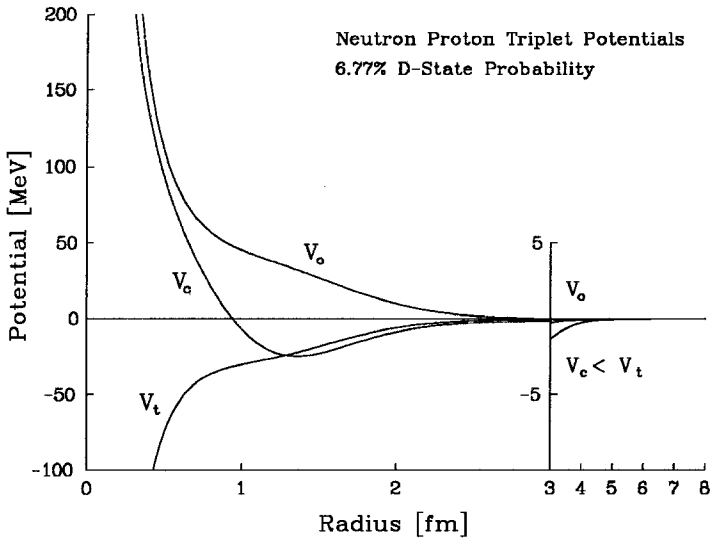


Fig. 13. Deuteron potentials to case (b)

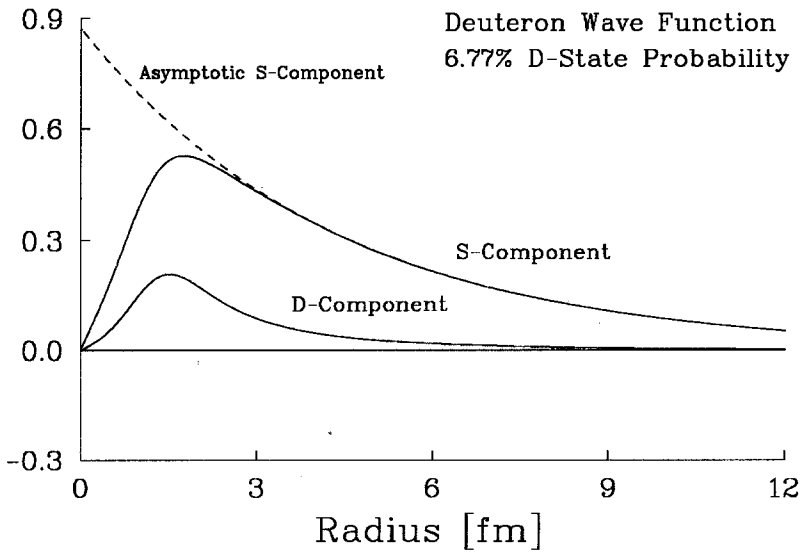


Fig. 14. Deuteron wave functions to case (b).

## 2.4 ${}^3PF_2$ -channel results

An other application shows inversion results for the  ${}^3PF_2$ ,  $T = 1$  channel based on data shown in Fig. 15.

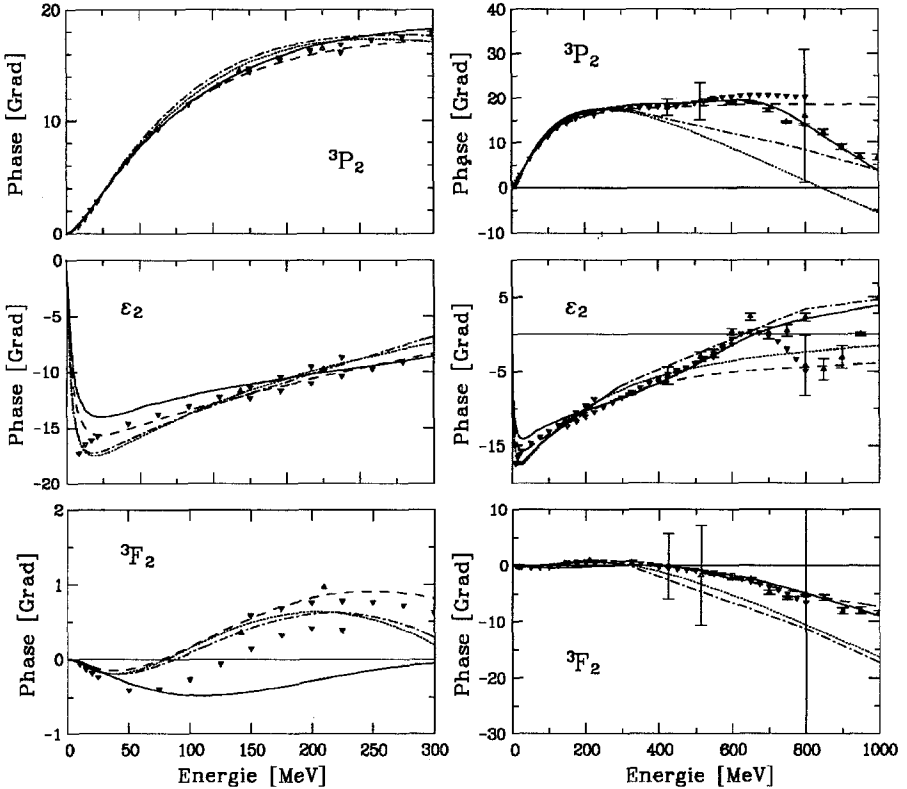


Fig. 15. Summary of  ${}^3PF_2$  channel data. Eigenchannel values are from the sources Virginia [16] (full), Nijmegen [22] (dashed), Saclay [18] (triangles), Arndt single energy data [16] (squares wit error bars), Bugg [17] (triangles with error bars), and OBEP phases from Paris [19] (dotted) and Bonn-B [21] (dash-dotted).

As the data show rather large uncertainties we obtain a band of inversion potentials. Even though this channel does not support any bound state, we find a very stable coupling potential  $V_{12}(r)$  for radii  $r > 0.8$  fm, see Figs. 16 and 17. More details about the tensor potential in this channel are shown in Fig. 18, where the genuine Paris and Nijmegen-3 tensor potentials are included for comparision. Our conclusion from these results is that the  $T = 1$  tensor potential is very well defined from existing data and the regularized Paris potential is in good agreement with our inversion results for all radii  $r > 0.6$  fm.

The Nijmegen-3 phase shifts are parametrized via Reid like local potentials

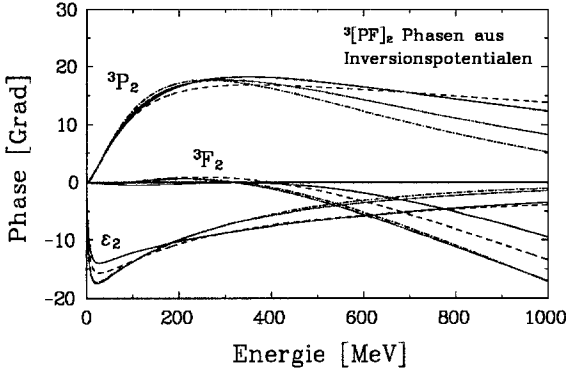


Fig. 16. Interpolated phase functions for  ${}^3PF_2$  channel to data below 300 MeV from Virginia [16] (full), Nijmegen-3 [22] (dashed), and OBEP Paris [19] (dotted), Bonn-B [21] (dash-dotted).

for proton-proton and proton-neutron data respectively [22]. The data fit is limited to subthreshold data and the potential thus extrapolates freely towards higher energies. We are following in our extrapolation more the trend in Arndt's phase shifts and find thus different potentials, see Fig. 19 and 20. This example shows, similar to Fig. 8, how *inversion* incorporates high energy phase shifts and how difficult it is for *direct* problem solutions in the  ${}^3PF_2$  channel [2].

## 2.5 Momentum space pictures

To solve the Lippmann-Schwinger equation for the  $t$ -matrix it is useful to have momentum space potentials

$$V_{\ell_1, \ell_2}^{S, J, T}(k, q) = V(k, q) = i^{\ell_1 - \ell_2} \int_0^\infty j_{\ell_1}(kr) V_{\ell_1, \ell_2}(r) j_{\ell_2}(qr) r^2 dr, \quad (41)$$

which are double Bessel Fourier transforms of the  $r$ -space potentials. Some potentials are already parametrized in momentum space [19, 21]. In Figs. 21 and 22 are shown nonlinear plots of momentum space potentials for the genuine Paris potential [19] and its inversion potential partner. These figures have  $0 < k, q < 50 \text{ fm}^{-1}$  as range and are thus reaching far beyond the on-shell momentum of  $0 < k < 2 \text{ fm}^{-1}$  range. Nevertheless, numerically this is an often used range in few body calculations and that is the reason for our choice for the display. The differences between the inversion (left) and genuine (right) potentials is the smooth high energy behavior induced by the asymptotic extrapolations of our phase shifts. Contrary to inversion produces the Paris potential a not realistic high energy behavior which signals a very repulsive inner core. The data by Arndt [16] and Saclay [18] show a flat high energy behavior of the phase shifts and we followed with our extrapolation closely the trend given by data and not the original Paris phase shifts. The momentum space potentials imply the same

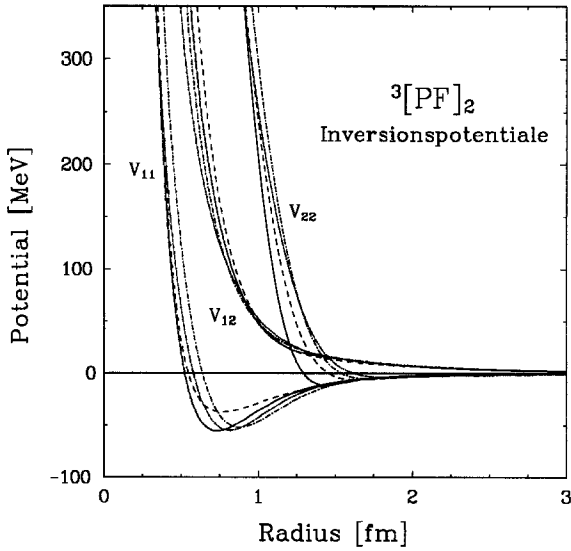


Fig. 17. Inversion potentials to  ${}^3PF_2$  channel data. Nomenclature follows Fig. 16.

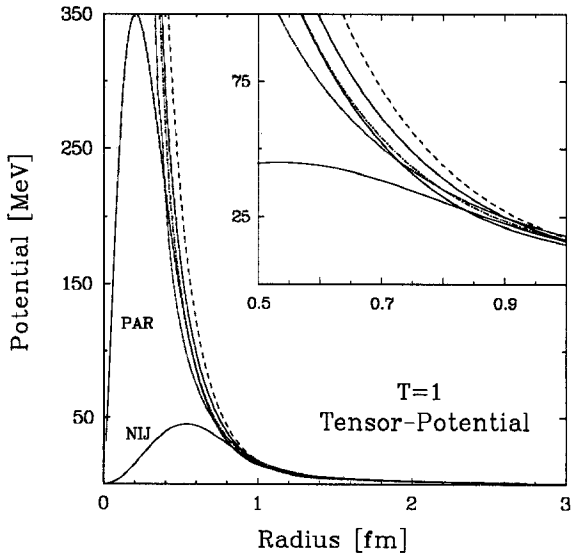
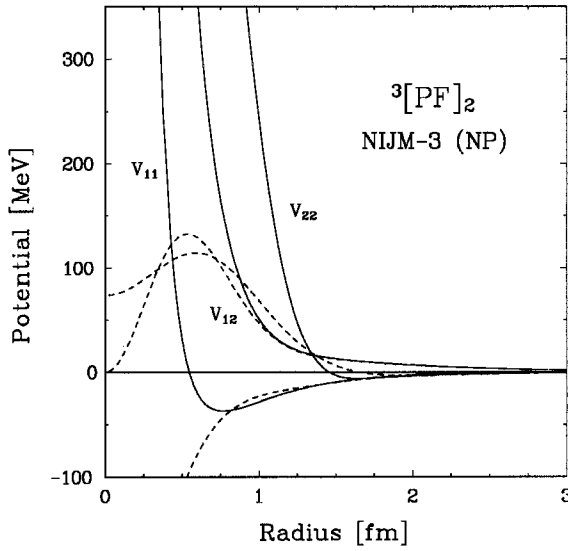
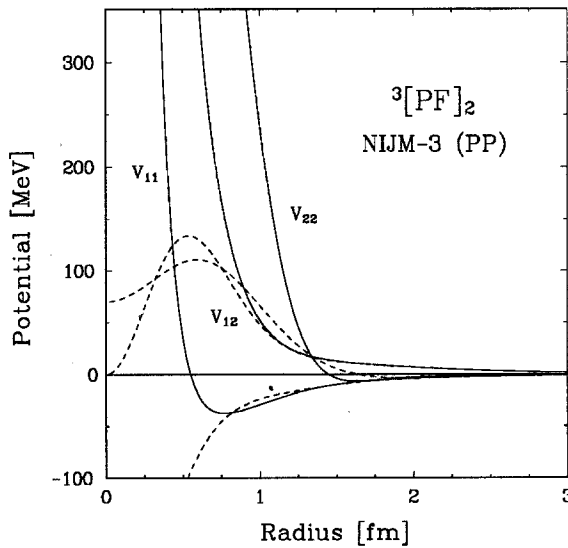


Fig. 18.  $T = 1$  tensor force extracted from Fig. 17 coupling potentials  $V_{12}$ . Also shown are the original  $T = 1$  tensor forces from Paris (PAR) [19] and Nijmegen-3 (NIJ) [22]. Line conventions follow Fig. 16.



**Fig. 19.** Potentials reproducing Nijmegen phase shifts in the coupled  $J = 2$  neutron-proton channel inversion (full), original Nijm-3 (dashed).



**Fig. 20.** Potentials reproducing Nijmegen phase shifts in the coupled  $J = 2$  proton-proton channel inversion (full), original Nijm-3(dashed).

phase shift for  $0 < E < 300$  MeV for inversion and Paris potentials but they differ above 300 MeV. There are now several new accelerator facilities in operation which will investigate just this region and we hope that inversion will also turn out to be useful in this energy domain as it is for energies below pion threshold.

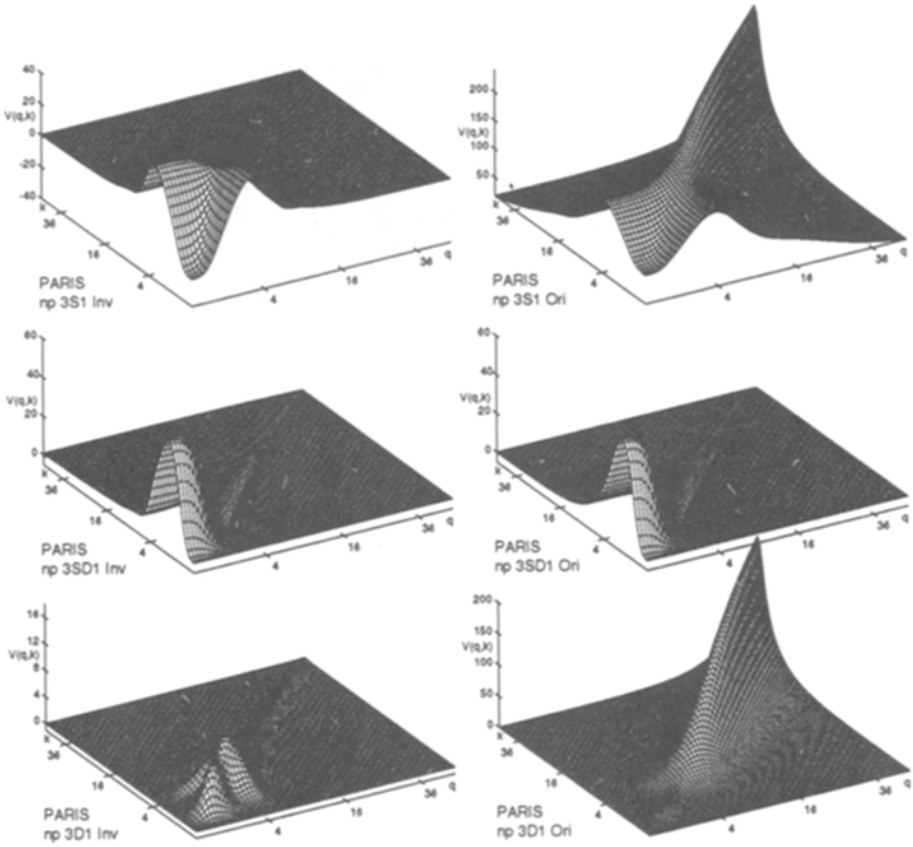


**Fig. 21.** Momentum-space pictures of nonlocal Paris potentials, inversion (left), original (right), in  ${}^3SD_1$  channel.

## Acknowledgement

We are indebted to Martin Küker, Martin Kröger and Mathias Sander to make some of their calculations available prior to publication. This work was supported in part by COSY, KFA-Jülich, GrantNr. 41126865.

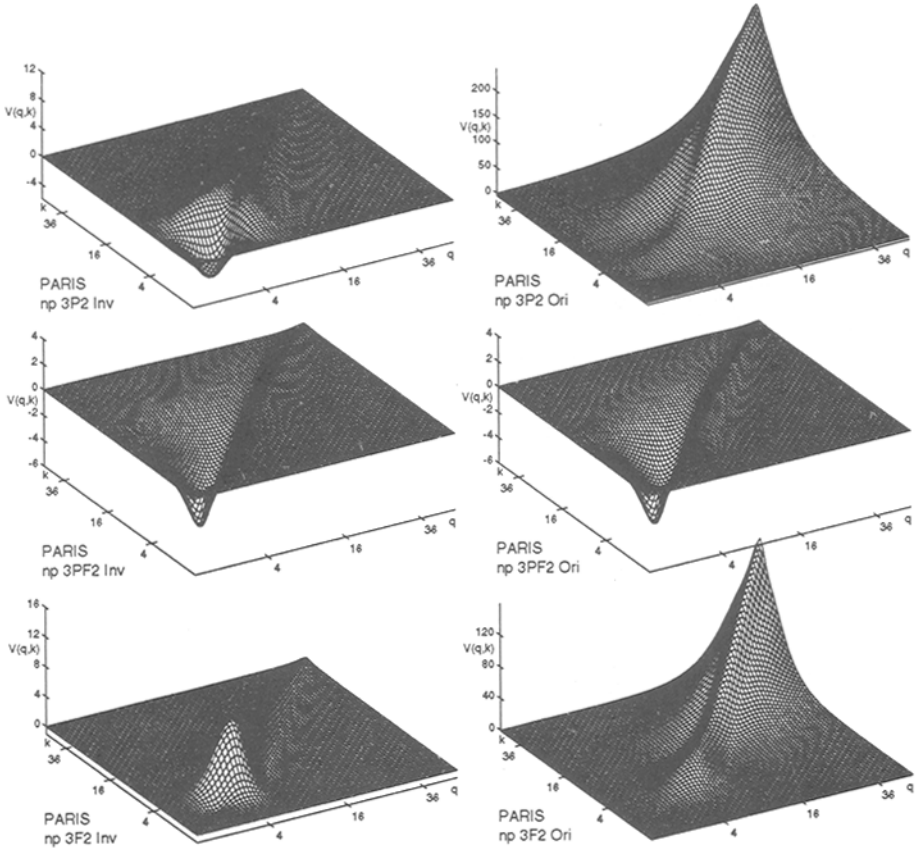


**Fig. 22.** Momentum-space pictures of nonlocal Paris potentials, inversion (left), original (right), in  ${}^3PF_2$  channel.

## References

1. K. Chadan and P.C. Sabatier, *Inverse problems in quantum scattering theory*, Springer, New York (1977), 2. Edition (1989)
2. H. Kohlhoff, M. Küker, H. Freitag and H.V. von Geramb, *Physica Scripta* **48**, 238 (1993)  
H. Kohlhoff, *Nukleon-Nukleon Potentiale und Quanteninversion der Streumatrix*, Thesis, Hamburg (1993)  
H. Kohlhoff, *Rationale Darstellungen der Nukleon-Nukleon S-Matrizen*, Diplomarbeit, Hamburg (1989)
3. Th. Kirst, *Nukleon-Nukleon Potentiale aus der Inversion*, Thesis, Hamburg (1989)
4. Th. Kirst et al., *Phys. Rev.* **C40**, 912 (1989)  
Th. Kirst, H. Kohlhoff and H.V. von Geramb, *Quantum Inverse Scattering Theory and Nucleon Nucleon Potentials*, Proc. R.C.P. 264, *Problemes Inverses* (1989), Montpellier (France), Springer Verlag (1990)

- Th. Kirst, *Theoretische Grundlagen und Algorithmen zur Konstruktion des Deuteron Potentials aus der Inversion*, Internal Report, Hamburg (1991)
5. G.A. Baker and P. Graves-Morris, *Padé-Approximants, Part I: Basic Theory, Part II: Extensions and Applications*, Encyclopedia of Mathematics and its Applications, Vols. 13 and 14, Addison-Wesley (1981)
  6. I. Gohberg and N. Krupnik, *One-dimensional linear singular integral equations*, OT53 and OT54, Birkhäuser (1992)
  7. V. Troitsky, *see contribution to this conference*
  8. M. Coz, *see contribution to this conference*
  9. M. Jetter, H. Kohlhoff, H. Freitag and H.V. von Geramb, *Physica Scripta* **48**, 229 (1993)  
M. Jetter, *Nukleon-Nukleon, Nukleon-Antinukleon Bremsstrahlung im Potential Modell*, Thesis, Hamburg (1993)
  10. B. Gibson, Theory Division, Los Alamos, *private communication*
  11. W. Glöckle, Universität Bochum, *private communication*
  12. J. Wambach, *see contribution to this conference and cited references*
  13. M. Küker, *Nukleon-Nukleon Inversions Potentiale für pp- und np-Streuung*, Diplomarbeit, Hamburg (1992)
  14. M. Sander, *Nukleon-Nukleon Potentiale für die Praxis*, Diplomarbeit, Hamburg (1993)
  15. A.K. Louis, *Inverse und schlecht gestellte Probleme*, Teubner, Stuttgart (1989)
  16. R.A. Arndt and L.D. Roper, *Nucleon-nucleon partial-wave analysis to 1 GeV*, *Phys. Rev.* **D28**, 97 (1983)  
R.A. Arndt, J.S. Hyslop III, and D.L. Roper, *Nucleon-nucleon partial-wave analysis to 1100 MeV*, *Phys. Rev.* **D35**, 128 (1986)  
R.A. Arndt, *Nucleon-nucleon partial-wave analysis to 1.6 GeV*, *Phys. Rev.* **D45**, 3995 (1992)  
R.A. Arndt, *Nucleon-nucleon partial-wave analysis to 1.6 GeV*, *Phys. Rev.* **D45**, 3995 (1992)  
R. Arndt, SAID with FA91 solution, VPI (1993)
  17. D.V. Bugg, *np phase shifts, 142 to 800 MeV*, *Phys. Rev.* **C41(6)**, 2708 (1990)
  18. J. Bystricky et al., *Nucleon-Nucleon phase shift analysis*, *J. Physique* **48**, 199 (1987)
  19. M. Lacombe et al., *Phys. Rev.* **C21**, 861 (1980)
  20. R. Machleidt, R. Holinde, and Ch. Elster, *The Bonn Meson-Exchange Model for the Nucleon-Nucleon Interaction*, *Phys. Rep.* **149(1)**, 1 (1987)
  21. R. Machleidt, *The Meson Theory of Nuclear Forces and Nuclear Structure*, *Adv. Nucl. Phys.* **149**, 189 (1989)
  22. J.R. Bergervoet et al., *Phys. Rev.* **C38**, 15 (1988), *ibid* **C41**, 1435 (1990)  
R.A.M. Klomp et al., *Few-Body-Systems*, *Suppl.* **6**, 105 (1992) and *Phys. Rev.* **C44**, R1258 (1991)  
V. Stoks and J.J. de Swart, *Phys. Rev.* **C47**, 761 (1993)  
The nucleon-nucleon Nijmegen-3 potential program code was made available by Dr. Vincent Stoks, *private communication* (1992)
  23. M. Jetter and H.V. von Geramb, *Nucleon-nucleon potentials and their test with bremsstrahlung*, submitted to *Phys. Rev.* (1993)
  24. R. Newton and T. Fulton, *Phys. Rev.* **107**, 1103 (1957)
  25. R. Newton and L.H. Scofield, *Phys. Rev.* **110**, 785 (1958)